The Pitzer Free Rotor Model for Nondegenerate Modes: Application to the Long-Range Behavior of Halogen Radical Reactions with Substituted Olefins

Mohamed Kharroubi and Pascal de Sainte Claire*

Laboratoire de Chimie Théorique, UMR6517, CNRS et Universités d'Aix-Marseille I et III, Avenue Escadrille Normandie-Niemen, Case 521, Marseille, 13397 Cedex 20, France

Received: March 29, 2002; In Final Form: February 20, 2003

While the Pitzer model had been used in the past with great success for degenerate internal motions, e.g., transitional bending motions in the recombination of hydrogen and methyl radicals, simpler models are often used in the treatment of nondegenerate modes, such as the transitional bending motions in the recombination reaction of hydrogen and choloromethyl radicals. In this work, highly detailed analysis of the Pitzer free rotor treatment for nondegenerate internal motions is presented. The addition reaction of a chlorine radical with 1,1,-dichloroethylene is used here for illustrative purposes. The reaction proceeds in two steps: the reactants reach a bridged intermediate that can dissociate back to reactants or yield the $^{\bullet}C_2H_2Cl_3$ adducts. Only the long-range part of the reaction was investigated in this paper. Electronic structure calculations were performed at the UQCISD(T)/6-31G**//UMP2/6-31G** level of theory, and canonical variational transition state theory rate constants were computed. In conclusion, it is shown that two different pathways lead to the bridged intermediate. Consideration of the forward and backward rate constants demonstrated that the more direct route to the bridged intermediate is favored kinetically.

Introduction

Specific treatments for barrierless reactions have been reported in the literature, such as the variational approach of transition state theory (VTST).[1,2] In this model, the transition state (TS) is located at the maximum of free energy along the minimum energy path (MEP).[3] Most VTST studies investigated were reactions where (1) the variational TS was short-range and transitional modes, i.e., the modes that change significantly along the path, were treated with the vibrator model[4,5] or (2) the variational TS was long-range and transitional modes were degenerate. In this case, the Pitzer free rotor model[6,7] was used with great success.[8] Although the Pitzer model is more complex for a species with many coupled nondegenerate internal rotors, a simple expression has been recently[9] provided for the specific case of two three-dimensional internal rotors.

In this paper, the addition reaction of a chlorine radical to 1,1-dicloroethylene is used for illustrative purposes. Free radical addition reactions to substituted alkenes represent a key step in polymerization[10−12] and telomerization processes[13−21] in combustion kinetics,[22] atmospheric chemistry,[23−25] and biological mechanisms.[26,27] One major challenge consists of fully understanding the regioselectivity of these reactions[28−30] in order to design regularly patterned polymers. The kinetic control of propagation and telogen transfer rate constants is another important issue in this field. Moreover, recent developments of telogen addition to halogenated monomers encouraged theoretical investigations at the microscopic level.[13]

This paper is organized as follows: first, detailed description and analysis of the Pitzer free rotor model is presented for the addition reaction of a radical species to disubstituted olefins. Although olefins with C_{2v} symmetry were chosen for simplicity purposes, the treatment is similar for asymmetric species. Second, the above model was used to compute rate constants for the addition reaction of a chlorine radical to 1,1-dichloroethylene. An important feature for this type of reaction is the presence of a bridged intermediate on the MEP.[4,31−36] In this work, we focused on the long-range part of this reaction.

The Kinetic Model

In this section, a model that allows computation of rate constants for very long range barrierless bimolecular association reactions (X + A → products) is presented. The canonical variational transition state theory (CVTST) has proven to be extremely useful and accurate for the treatment of such reactions, especially radical/radical recombination and ion/molecule association reactions.[37,38]

I. The CVTST Rate Constant. Let atom X and species A be the fragments and *N* the total number of atoms. The CVTST rate constant can thus be written[2] as

$$k_{\mathrm{CVTST}} = \frac{k_{\mathrm{B}}T}{h}\frac{Q^{\ddagger}}{Q_{\mathrm{X}}Q_{\mathrm{A}}}\mathrm{e}^{-E_{\mathrm{o}}/k_{\mathrm{B}}T} \qquad (1)$$

where Q_i are molecular partition functions ("‡" stands for TS). Mode separability is assumed and thus global molecular partition functions are written as products of molecular partition functions for the different degrees of freedom, i.e., translational, rotational, vibrational, and electronic. Nuclear partition functions are assumed to be equal to unity. E_{o} is the electronic energy difference between transition state and reactants, including the zero-point energy. A contribution to zero-point energy arises

* Corresponding author. Present address: Laboratoire de Photochimie Moléculaire et Macromoléculaire, UMR CNRS 6505, ENS Chimie de Clermont-Ferrand, Université Blaise Pascal, F-63177 Aubière Cedex, France.

10.1021/jp0258614 CCC: $25.00
Published on Web 05/13/2003

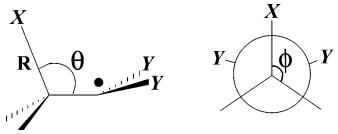

Figure 1. Principal geometric parameters used in this work. θ and φ motions were identified with internal rotations of the axis that connected the incoming X atom and the $C_2H_2Y_2$ center-of-mass.

from conserved (i.e., nontransitional) modes only. The terms k_B and h are the usual Boltzmann and Planck constants, and T is the temperature (room temperature was used in the present work).

In proceeding from reactants to products, three modes are created, one of which is the reaction coordinate. The reaction coordinate was projected out of the mass-weighted Cartesian Hessian matrix, which after diagonalization yielded $3N - 7$ frequencies, i.e., the modes that are orthogonal to the reaction coordinate. Among these $3N - 7$ vibrational frequencies, $3N - 9$ do not vary significantly between the TS and the reactants because of the very long range character of the TS. They are the conserved modes. The remaining two frequencies (the transitional modes) changed between 0 and some finite value at the TS. They are labeled θ and φ. Therefore, the ratio of TS and reactants vibrational partition functions is

$$\frac{q_{\text{vib}}^{\ddagger}}{q_{\text{vib}}^{\text{A}}} = q_{\theta}^{\ddagger}\, q_{\varphi}^{\ddagger} \tag{2}$$

In eq 2, the cancelation of the conserved modes was assumed. If this hypothesis is not verified, the conserved modes should be included in the ratio of vibrational partition functions.

Since X is an atom, only the translational and electronic components of the molecular partition function contribute to the rate constant:[39]

$$k_{\text{VTST}} = \frac{k_B T}{h}\frac{1}{q_{\text{trans}}^{\mu}} q_{\theta}^{\ddagger}\, q_{\varphi}^{\ddagger} L \left(\frac{I_1^{\ddagger} I_2^{\ddagger} I_3^{\ddagger}}{I_1^{\text{A}} I_2^{\text{A}} I_3^{\text{A}}}\right)^{1/2} \frac{q_{\text{elec}}^{\ddagger}}{q_{\text{elec}}^{\text{X}}\, q_{\text{elec}}^{\text{A}}} \mathrm{e}^{-E_o/k_B T} \tag{3}$$

In eq 3, q_{trans}^{μ} is the translational partition function for a species of mass μ; μ is the reduced mass of X and A; L is the ratio of the rotational symmetry numbers for TS and A (i.e., the reaction path degeneracy); and the fraction in parentheses is the ratio of the respective principal moments of inertia. $q_{\text{elec}}^{\ddagger}/q_{\text{elec}}^{\text{X}} q_{\text{elec}}^{\text{A}}$ is the ratio of the respective electronic partition functions.[40]

II. Transitional Modes Treatment. Different approaches have been used in the literature for the treatment of transitional modes, one of which is the free rotor treatment.[41−43] Such a model accounts for fundamental changes in the character of the transitional modes. Let us consider the model reaction where A is a disubstituted olefin:

$$^{\bullet}\text{X} + \text{CH}_2{=}\text{CY}_2 \rightarrow \text{CXH}_2{-}^{\bullet}\text{CY}_2$$

In the associated species, the transitional modes become nondegenerate X−C−C bending modes. They are described in Figure 1: θ motion conserves the C_s symmetry, while φ motion breaks it. To a good approximation, and provided the frequencies for these modes are large enough, such degrees of freedom can be represented by oscillator partition functions. However, because the X···C distance is large at the TS, the θ and φ motions are better represented by free internal rotations than vibrations. The axes for these internal rotations originate at the center-of-mass of $C_2H_2Y_2$. Such a treatment becomes increasingly important as long as one of the following is fulfilled: (1) the interfragment distance at the TS is large (in general, the lower the temperature the larger this distance for radical/radical association reactions) or (2) if the temperature is high, the harmonic oscillator partition function does not go to the correct asymptotic limit, since it behaves as T, whereas the monodimensional rotational partition function is proportional to $T^{1/2}$. Truhlar[44] proposed an empirical switching function that allowed the partition function to change continuously from a vibration to a free (or hindered) internal rotation. This model was not used here since the addition reactions in our work were long-range and the transitional modes were expected to behave much like free rotations.

Thus the product of internal rotation partition functions can be written as

$$q_{\theta}^{\ddagger}\, q_{\varphi}^{\ddagger} = \frac{8\pi^2 k_B T}{\sigma h^2}(I_{\theta} I_{\varphi})^{1/2} \tag{4}$$

where I_{θ} and I_{φ} are reduced moments of inertia for the θ and φ internal rotations, respectively. Since $C_2H_2Y_2$ has C_{2v} symmetry, I_{θ} and I_{φ} are not degenerate. In eq 4, $\sigma = 1$ is the symmetry number for this two-dimensional internal rotation. Next we describe the procedure that was used to obtain I_{θ} and I_{φ}.

III. Computation of the Reduced Moments of Inertia I_{θ} and I_{φ}. The free rotor model has been used in studies where the transition states were symmetric tops.[8] In this case, Pitzer and Gwinn[6] were able to provide a simple analytic expression for I_{θ} and I_{φ} (eq 5):

$$I_{\theta} = I_{\varphi} = I_{\text{A}}\left(1 - \frac{I_{\text{A}}}{I_{\text{X}\cdots\text{A}}}\right) \tag{5}$$

where I_{A} and $I_{\text{X}\cdots\text{A}}$ are the degenerate principal moments of inertia for species A and TS, respectively. The symmetric top nature of the TS implies that A is a symmetric top as well (or a spherical top). In the limit of the infinite X···A separation, eq 5 reduces to $I_{\theta} = I_{\varphi} = I_{\text{A}}$, i.e., internal rotations become the degenerate overall rotation of species A and the reaction coordinate becomes X relative translation. In eq 5, provided the X···A distance is sufficiently large, $I_{\text{X}\cdots\text{A}}$ can be approximated by $\mu r_{\text{X}\cdots\text{A}}^2$, where μ is the reduced mass of X and A, and $r_{\text{X}\cdots\text{A}}$ is the distance between X and A center-of-mass. In the third of a series of papers, Kilpatrick and Pitzer[7] showed how I_{θ} and I_{φ} could be exactly calculated for asymmetric species with many coupled internal rotors. This more exact method will be used here. The computation of I_{θ} and I_{φ} in the most general case is now briefly stated. A more detailed description can be found in refs 7 and 9.

First, define a fixed frame in the molecule, such as the C−C bond in our illustrative example, and any two axes orthogonal to each other and to this bond. Then define the internal rotors. X is undergoing two kinds of internal rotations (see Figure 1). The full kinetic energy matrix is then written down for this system in the fixed reference frame. The overall rotation is decoupled from overall translation by setting the origin at the system's center-of-mass. The kinetic energy matrix is now block diagonal. The first block is for overall translation of the species, and the second block comprises overall rotation, internal rotations, and their respective coupling terms. By further diagonalizing this second block about its three overall rotation diagonal elements, one is left with the internal kinetic energy matrix, decoupled from overall rotation. Its diagonal

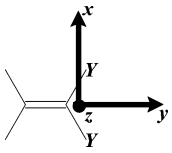

Figure 2. Principal axes of inertia *x*, *y*, and *z* for the $C_2H_2Y_2$ molecule. The origin is at the $C_2H_2Y_2$ center-of-mass.

elements are the reduced moments of inertia for internal rotation, whereas the nondiagonal elements correspond to the coupling terms between internal rotors. The partition function for internal rotation was shown to be proportional to the square root of the determinant of the internal kinetic energy matrix for the system.[45] In the work presented here, θ and φ internal rotations are orthogonal, thus already decoupled from one another, and the internal kinetic energy matrix is diagonal with elements I_θ and I_φ. I_θ and I_φ are computed along the MEP, and thus depend on $r_{X\cdots A}$, the interfragment distance, and other internal variables. In ref 7, internal rotors were off-balance in only one direction: *z* is the direction of the axis for internal rotation, the hindered rotor center-of-mass being in the *xz* plane, and thus contributing no *y* off-balance kinetic coupling. The most general procedure for internal rotation decoupling was programmed in our laboratory and used thereafter. In addition, the general expression of the internal kinetic energy matrix is given in the appendix.

For X···A symmetric top species, $I_\theta(r_{X\cdots A} = \infty) = I_\varphi(r_{X\cdots A} = \infty) = I_A$. This is generally not the case for asymmetric species. Let I_x^A, I_y^A, and I_z^A be the principal moments of inertia of $C_2H_2Y_2$, the axes of which are represented in Figure 2. C_s symmetry is conserved throughout the reaction. Thus, the incoming X atom lies in the *yz* plane. Moreover, since the geometries of fragments are similar to those of their infinite separations, two variables only, for example, $r_{X\cdots A}$ (the distance between the chlorine radical and A center-of-mass) and the attacking X−C−C angle θ change along the MEP (one can choose another set of variables, such as an interatomic distance and θ). Therefore, I_θ and I_φ are functions of $r_{X\cdots A}$ and θ only. It is easily seen (since X is in the *yz* plane) that, for $r_{X\cdots A}$ fixed, I_θ does not depend on θ (the axis for θ internal rotation is in the *x* direction). This means that, in the limit of infinite separation, I_θ approaches I_x^A, the principal axis for overall rotation of A in the *x* direction (see Figure 2 for the definition of *x*, *y*, and *z*). However, I_φ depends on both $r_{X\cdots A}$ and θ. Therefore, for infinite separations, only when the axis that connects the chlorine and A center-of-mass exactly matches *z* does I_φ approach I_z^A, the principal moment of inertia of A in the *z* direction. Similarly, only when the axis that connects the chlorine and A center-of-mass matches exactly *y* does I_φ approach I_y^A, the principal moment of inertia of A in the *y* direction. Thus, in the limit of infinite fragment separation, $I_\theta(r_{X\cdots A} = \infty)$ is equal to I_x^A, whereas $I_\varphi(r_{X\cdots A} = \infty,\theta)$ is different from both I_z^A or I_y^A.

In ref 9, Robertson et al. showed that the product of external and internal classical partition functions is proportional to $(\mu r_{X\cdots A}^2)^2 I_x^A I_y^A I_z^A$ (see above for the definition of variables). This expression is exact in the specific case of two three-dimensional internal rotors. For our model reaction, A is undergoing one two-dimensional internal rotation; thus, I_θ and I_φ are related to $\mu r_{X\cdots A}^2$ through eq 6:

$$I_\theta I_\varphi I_1^\ddagger I_2^\ddagger I_3^\ddagger = (\mu r_{X\cdots A}^2)^2 I_x^A I_y^A I_z^A \qquad (6)$$

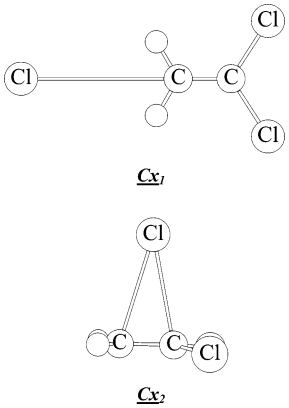

Figure 3. Geometries of the Cx_1 and Cx_2 intermediates. See also Table 1.

As expected, a perfect agreement was reached between both methods.[46] In ref 9, a similar agreement was obtained for the $H+CH_3$ addition reaction (results were labeled CFR and CFTST-FR). In standard VTST calculations, external rotational degrees of freedom at the TS are generally assumed decoupled from internal rotation. In this case, eq 6 clearly shows that the product $I_\theta I_\varphi$ should not be simply replaced by $\mu r_{X\cdots A}^2$.[47]

Application to the Model Reaction $^\bullet Cl + CH_2{=}CCl_2 \rightarrow CClH_2{-}^\bullet CCl_2$

In this section, the above method is used to compute rate constants for the reaction of chlorine radicals with 1,1-dichloroetylene. High-level electronic structure calculations (section I below) were performed to obtain a reliable potential energy surface (PES), and canonical variational transition state theory rate constants are computed and discussed in section II.

I. Electronic Structure Calculations. The reactivity of substituted olefins toward radical species has been extensively studied with theoretical methods. In recent work, electronic structure calculations were performed with the density functional theory (DFT).[48−52] However, in some cases, a bridged intermediate could not be obtained on the DFT PES.[32] More generally, correlated wave functions are needed because the alkene triplet state contributes in a significant manner to the MO wave function.[53−55] Thus, configuration interaction (CI) methods seem to be adequate to obtain accurate potential energy surfaces for the type of reaction investigated here.[31−33,56−61]

In this work, electronic structure calculations were performed at the UQCISD(T)/6-31G**//UMP2/6-31G** level of theory with the Gaussian series of programs.[62] Geometries were optimized with the second-order Møller−Plesset perturbation theory and the 6-31G** basis set (polarization basis functions were used for both hydrogen and heavy atoms). Single-point calculations were carried out with the above geometries and the quadratic CI method (corrections for single, double, and triple excitations are included). Polarized Hamiltonians, i.e., unrestricted calculations, were used throughout.

Several minima were found on the UMP2/6-31G** PES, among which are the product isomer species $CH_2Cl-{}^\bullet CCl_2$ and $^\bullet CH_2-CCl_3$, and two long-range intermediates Cx_1 and Cx_2 (see Figure 3). In Cx_1, the incoming chlorine radical and the carbon atoms are aligned. Cx_1 is stabilized by long-range dipole/dipole-induced interactions and has C_{2v} symmetry. Cx_2 is a bridged intermediate with C_s symmetry and, from previous calculations, was expected on the MP2 PES.[4,31−35] Energies and relevant geometrical parameters of the above species are given in Table 1 and Figure 3. Thus, the reactants and the bridged

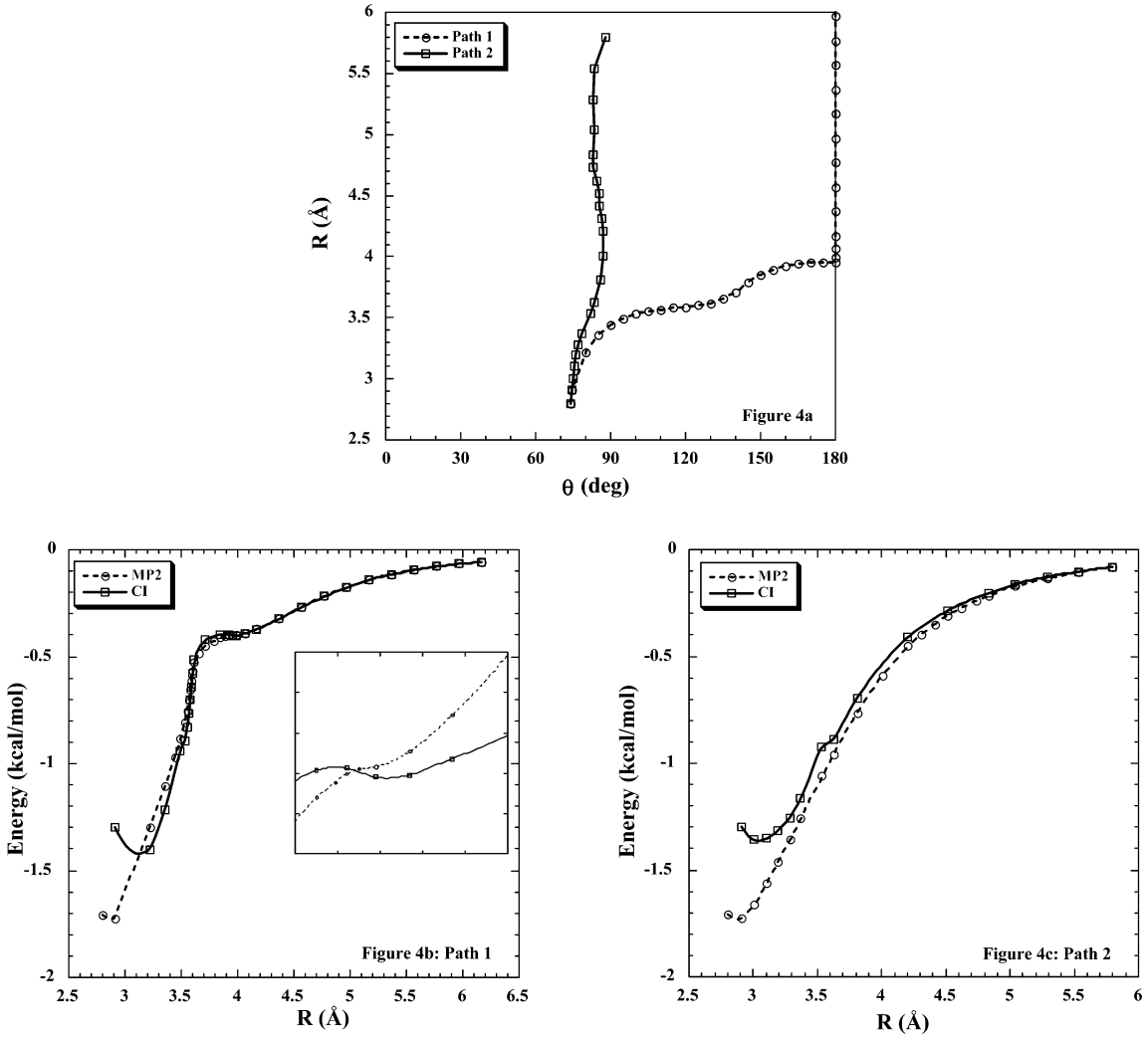

Figure 4. Minimum energy paths (MEPs) between reactants and the bridged intermediate Cx_2 (see text). In Figure 4a, the dependence of R on θ is displayed for the MEPs. In parts b and c, the UMP2/6-31G** and UQCISD(T)/6-31G**//UMP2/6-31G** energies are plotted against the Cl−CH_2 distance (R, see Figure 1) for paths 1 and 2, respectively.

TABLE 1: Electronic Structure Calculation Results[a]

species	E(MP2)[b]	E(CI)[c]	R[d]	θ[d]	$R_{C=C}$[d]
Cx_1[e]	−0.40	−0.40	3.951	180.0	1.334
Cx_2[e]	−1.73	−1.23	2.866	74.2	1.351
$ClCH_2-{}^{\bullet}CCl_2$	−19.4	−18.4	1.802	113.2	1.478
${}^{\bullet}CH_2-CCl_3$	−7.81	−5.54	1.798	(109.6)[f]	1.476

[a] Distances are in angstroms, angles in degrees, energies in kcal/mol. The reference energy is that of the separated reactants at the respective level of theory. [b] Electronic energy at the UMP2/6-31G** level of theory. [c] Electronic energy at the UQCISD(T)/6-31G**//UMP2/6-31G** level of theory. [d] R is the Cl···CH_2 interfragment distance, θ the Cl···CH_2═CCl_2 attacking angle (see Figure 1), and $R_{C=C}$ the carbon/carbon bond length ($R_{C=C}$ = 1.334 Å for the reactant species). [e] Cx_1 is the long-range species with the linear Cl···C═C structure, whereas Cx_2 is the bridged intermediate. [f] The value for the Cl−$CCl_2-{}^{\bullet}CH_2$ angle is listed in parentheses (in place of the Cl−$CH_2-{}^{\bullet}CCl_2$ angle).

intermediateare connected through two different MEPs. The overall reaction scheme is shown below:

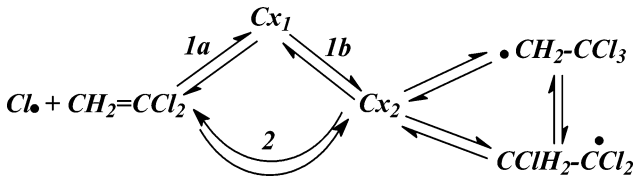

Because the reactive pathways investigated here are barrierless, the minimum energy path (MEP)[63,64] was identified with the reaction path. At large interfragment distances, the reaction coordinate is mainly a function of the Cl···CH_2 distance and the attacking Cl···CH_2═CCl_2 angle, R and θ, respectively (see Figure 1). The MEP was obtained by fixing the distinguished coordinate R while optimizing all the other degrees of freedom (however, the reaction coordinate between Cx_1 and Cx_2 more likely resembled θ, which was, for this part of the MEPs only, the distinguished coordinate. See Figure 4a where the dependence of R on θ is displayed). The MEPs between reactants and the bridged intermediate are represented in Figure 4b,c and are labeled paths 1 and 2, respectively. In Figure 4b, the plateau region around R = 4 Å characterizes the region of the long-range Cx_1 structure. Normal-mode analysis (harmonic approximation) showed that Cx_1 was a true local minimum at the MP2 level, and single-point calculations at the CI level (i.e., UQCISD(T)/6-31G**//UMP2/6-31G**) confirmed this result (see inset in Figure 4b). Past theoretical investigations of radical addition reactions to substituted olefins assumed path 2 was the unique way to reach the bridged Cx_2 intermediate. Although the rate constants in paths 1 and 2 are quite different (see Kinetic Results Section below), it may be interesting in future work to see if Cx_1 can play an active role in the reaction (for example, in cases where the dipole moment of the olefin is large or where

the incoming radical is highly polarizable). However, thermal equilibrium is unlikely for such a shallow minimum, and the reactants will be considered to proceed to Cx_2 via a single-step process in path 1. The overall scheme may now be represented as follows:

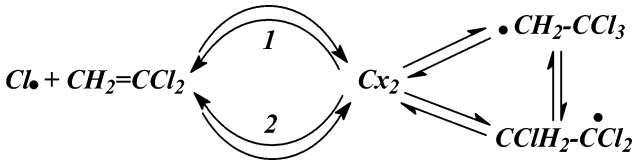

Two different elementary bimolecular processes may yield the bridged intermediate Cx_2. In path 1 (Figure 4b), the chlorine radical reacts collinearly to the carbon/carbon bond (with C_{2v} symmetry) and the reaction coordinate is mainly a function of R. Next, the chlorine radical shifts in the C_s plane until Cx_2 is reached (the reaction coordinate is mainly a function of R and θ). In path 2 (see Figure 4c), the incoming chlorine radical proceeds directly to the bridged intermediate (C_s symmetry is kept throughout the course of path 2). In accordance to what was found in another study,[32] Cx_2 was not found with the DFT method (various functionals were used with the 6-31G** basis set).

First, MP2 and CI calculations agree very well for interfragment distances larger than 3.2 Å. It will be shown further that the variational transition states are located in this region of the phase space and that MP2 level calculations adequately yield CVTST rate constants for paths 1 and 2. However, the discrepancy between the MP2 and CI results becomes sizable as Cx_2 progresses to the product radical species $^{\bullet}C_2H_2Cl_3$.

Last, the carbon/carbon bond length $R_{C=C}$ changes very little between reactants and Cx_2 (see Table 1). However, harmonic frequencies of some conserved modes in Cx_2 differed significantly from those in $C_2H_2Cl_2$ (in Cx_2, the carbon/carbon bond is part of a three-body bridged structure while it is purely olefin-like in $C_2H_2Cl_2$) and the conserved modes were included in the calculation of the rate constant (in eq 2).

The final reaction step ($Cx_2 \rightarrow {}^{\bullet}C_2H_2Cl_3$) was thoroughly investigated and is briefly discussed below. Results show that much higher level calculations than those performed here (i.e., large CASSCF calculations) are needed to obtain a potential energy surface free from spin-contamination. Moreover, this part of the reaction is of a much shorter range and the respective rate constants may be obtained with standard procedures.

The reaction of a chlorine radical with ethylene was recently shown[31] to proceed through a bridged intermediate ($^{\bullet}C_2H_4Cl$), which, in turn, could react and yield either of the identical isomers $^{\bullet}CH_2-CH_2Cl$ or $CClH_2-{}^{\bullet}CH_2$. It was shown that the chlorine shift from one carbon atom to the other proceeded preferentially through a two-step mechanism. $^{\bullet}CH_2-CH_2Cl$ went back to the bridged intermediate, which, in turn, reacted unimolecularly and yielded the other isomer $CH_2Cl-{}^{\bullet}CH_2$. The above indirect chlorine shuttling motion was shown to be thermodynamically favored with respect to the direct shuttling motion. In our work, one isomer is more stable (see Table 1). $CClH_2-{}^{\bullet}CCl_2$ and $^{\bullet}CH_2-CCl_3$ lie 18.4 and 5.5 kcal/mol, respectively, below the reactants, in agreement with experimental results.[65,66] Only $Cx_2 \rightarrow CClH_2-{}^{\bullet}CCl_2$ was examined in this work. However, as shown below, more adequate electronic structure methods are needed for this part of the reaction.

A tight transition state that connected Cx_2 and $CClH_2-{}^{\bullet}CCl_2$ was found at the UMP2/6-31G** level. However, the obtained structure was highly spin-contaminated. This is a well-known artifact for addition reactions of the type investigated here, and spin-projected calculations (and/or larger basis sets) are often used to circumvent the problem.[33,36,56] However, single-point PMP2/6-31G**//UMP2/6-31G** calculations lowered the energy of the UMP2 TS below that of Cx_2 (see Figure 5). It should be noted that Cx_2 is not spin-contaminated and is a true local minimum at the UMP2/6-31G** level. Therefore, the geometry of the actual TS that connected Cx_2 and the most stable isomer product ought to differ significantly from that obtained at the UMP2 level; thus, multireference CI or CASSCF methods are necessary[59,67] to obtain accurate rate constant for these processes. Other possibilities include full optimizations at the UQCISD(T) level.[31,32] However, Hessian matrix diagonalizations are unpractical for many heavy atom systems. Such calculations are beyond the subject of this work and will not be presented here.

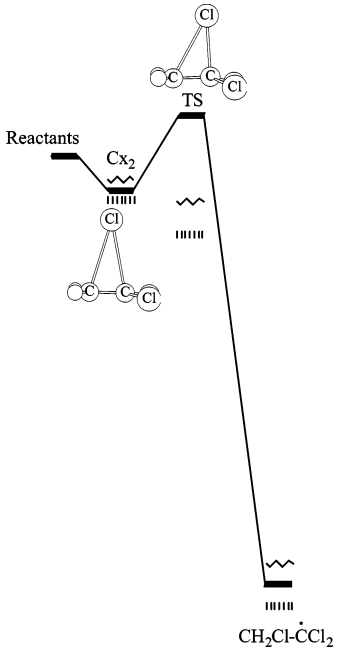

Figure 5. Energy levels of the reactants ($^{\bullet}Cl+CH_2{=}CCl_2$), the bridged intermediate (Cx_2), the more stable product isomer ($ClCH_2-{}^{\bullet}CCl_2$), and the transition state (TS) between Cx_2 and $ClCH_2-{}^{\bullet}CCl_2$ at different levels of theory. The geometries of Cx_2 and the TS at the UMP2/6-31G** level are shown. All geometries were optimized at the UMP2/6-31G** level (bold solid). PMP2 (hashed) and UQCISD(T) (wavy) results are single-point calculations on the respective UMP2 geometries (see text). Actual relative scaling is shown.

II. Kinetic Results. Free energies $\Delta G(R)$ were computed for the geometries obtained at the UMP2/6-31G** level on the MEPs (electronic energies were those calculated at the UQCISD(T)/6-31G**//UMP2/6-31G** level). The maximum value for ΔG was identified with the free energy of reaction for the respective pathway. The corresponding angle and bond distance at the variational TS are labeled $\theta^{\ddagger}$ and $R^{\ddagger}$, respectively. Finally, the principle of microscopic reversibility allowed calculations of the reverse rates in paths 1 and 2 (the θ and φ motions in Cx_2 were treated with the nondegenerate free rotor model). The results are shown in Table 2.

The mechanism is similar to the addition reaction of a chlorine atom to ethylene. Reactants proceed rapidly to a bridged intermediate on the reaction path, which, in turn, yields products or returns back to reactants. Experimental rates of 8.4 and 7.5×10^{13} cm^3/mol/s were reported for the addition reaction of chlorine radicals to 1,1-dichloroethylene.[35,68] This result was

TABLE 2: Canonical Variational Transition State Properties for Paths 1 and 2 (See Figure 4) and Rate Constants

	$R^{\ddagger}$ [a]	$\theta^{\ddagger}$ [a]	$V^{\ddagger}$ [b]	k^c	$k_{reverse}$ [c]
path 1	3.555	105	−0.829	9.0	4.23
path 2	4.515	85.4	−0.285	37.8	56.8

[a] $R^{\ddagger}$ is the Cl···CH_2 distance at the TS in Å, while $\theta^{\ddagger}$ is the Cl···CH_2−CCl_2 angle at the TS in degrees (see Figure 1). [b] $V^{\ddagger}$ is the classical potential energy at the TS with respect to reactants in kcal/mol. [c] k and $k_{reverse}$ are the forward and backward CVTST rate constants in units of 10^{13} cm^3/mol/s and 10^{13} s^{-1}, respectively. Standard reference state is 1 mol/L.

shown to be a good approximation of the high-pressure limit rate constant. Provided k_3 (see reaction scheme below) is smaller than $k_{-1} + k_{-2}$, the results in Table 2 (i.e., $k_1 \ll k_2$ and $k_{-1} \ll k_{-2}$) clearly show that path 2 is the most favored route to the bridged intermediate and that the chemical equilibrium between reactants and Cx_2 may be represented by a unique step, path 2

$$^{\bullet}Cl + CH_2{=}CCl_2 \underset{k_{-2}}{\overset{k_2}{\rightleftharpoons}} Cx_2 \xrightarrow{k_3} \text{products}$$

Here, k_3 is expected to be much smaller than $k_{-1} + k_{-2}$ since the unimolecular rearrangement from Cx_2 to products involves important electronic and geometric changes. This is not the case for the long-range part of the reaction. Finally, it is necessary that k_{-1} be much smaller than k_{-2} to rule out path 1 in the mechanism. Otherwise, the reactants would go to Cx_2 in path 2 and they return back to reactants in path 1. The reaction scheme would then have been

$$^{\bullet}Cl + CH_2{=}CCl_2 \underset{k_{-1}}{\overset{k_2}{\rightleftharpoons}} Cx_2 \xrightarrow{k_3} \text{products}$$

Moreover, the reverse process in path 1 was favored on thermodynamic grounds over that in path 2 (see $V^{\ddagger}$ values in Table 2).

Finally, the most recent work[68] reported a rate constant (7.5×10^{13} cm^3/mol/s) that is much smaller than k_2 in Table 2 (37.8×10^{13} cm^3/mol/s). In ref 68, the disappearance of the olefin species R is monitored and compared with that in a reference reaction (T, k_{ref}), e.g., the addition reaction of chlorine atoms to ethylene. The rate constants k are then fit from a plot of $\ln[R_o/R_t]$ versus $\ln[T_o/T_t]$:

$$\ln[R_o/R_t]/\ln[T_o/T_t] = k/k_{ref} \tag{7}$$

That is, experimental rates measure the overall decay of the olefin species. In our work, the overall disappearance of the olefin species may be represented by $k = k_2k_3/k_{-2}$ (a steady-state approximation for Cx_2 is assumed) and k_{-2} greater than k_3 results in apparent slower decay of the reactants, in agreement with experimental results.

Conclusion

The Pitzer free rotor expression was thoroughly discussed and used to model the transitional modes in the reactions of atoms and disubstituted olefins. Equation 6 shows that a simple expression can be used to compute reduced moments of inertia for nondegenerate transitional modes. Second, the rate constant for chlorine radical addition with 1,1-dichloroethylene was calculated with the variational transition state theory model. The addition reaction of a halogen radical to halogen-substituted olefins is characterized by a two-step mechanism. First, the reactants form a bridged intermediate that could in turn either step back to reactants, or yield products. Two conclusions arose from our results: (1) the collinear route (path 1) to the bridged intermediate can be neglected with respect to the more direct path (path 2) on the basis of respective rate constants, and (2) significant amount of the bridged intermediate goes back to reactants. This results in a slower apparent reactant decay.

Acknowledgment. The authors thank Professor M. Roche for valuable discussions and the Elf-Atochem company for financial support.

Appendix

In ref 7, clarity prompted the authors to give the internal kinetic energy matrix **S** for a system with internal rotors that were off-balance in only one direction. The most general expression for **S** (which was used in our Fortran program for the general computations of the moments of inertia) is given here. The variable designation is consistent with ref 7: M is the total mass, U_k^q the off-balance factor of internal rotor k in the q direction, A_k the moment of inertia for internal rotor k about its internal rotation axis, β_{k1}^q the kinetic energy matrix coupling term between the q component of overall rotation and internal rotation or rotor k. The expression for β_{k1}^q is given in ref 7. Finally, $\beta_{kk'}^z$ is the cosine of the angle between the z-axis of the k and k′ internal rotors. All internal rotors rotate about their own z-axis. The general expression for **S** is then

$$\mathbf{S} = \begin{pmatrix} A_1 - K_{11} & \beta_{12}^z - K_{12} & \beta_{13}^z - K_{13} & \dots & \dots \\ \beta_{12}^z - K_{12} & A_2 - K_{22} & \beta_{23}^z - K_{23} & \dots & \dots \\ \beta_{13}^z - K_{13} & \beta_{23}^z - K_{23} & A_3 - K_{33} & \dots & \dots \\ \dots & \dots & \dots & \dots & \dots \\ \dots & \dots & \dots & \dots & \dots \end{pmatrix} \tag{8}$$

where

$$K_{ii} = \frac{1}{M}(U_i^{x^2} + U_i^{y^2} - 2U_i^x U_i^y[\alpha_{i0}^{yx}\alpha_{i0}^{xx} + \alpha_{i0}^{yy}\alpha_{i0}^{xy} + \alpha_{i0}^{yz}\alpha_{i0}^{xz}]) \tag{9}$$

$$\begin{aligned} K_{ij} = \frac{1}{M}([\alpha_{i0}^{yx}U_i^x - \alpha_{i0}^{xx}U_i^y][\alpha_{j0}^{yx}U_j^x - \alpha_{j0}^{xx}U_j^y] + \\ [\alpha_{i0}^{yy}U_i^x - \alpha_{i0}^{xy}U_i^y][\alpha_{j0}^{yy}U_j^x - \alpha_{j0}^{xy}U_j^y] + \\ [\alpha_{i0}^{yz}U_i^x - \alpha_{i0}^{xz}U_i^y][\alpha_{j0}^{yz}U_j^x - \alpha_{j0}^{xz}U_j^y]) \quad \text{for } i \neq j \end{aligned} \tag{10}$$

In eqs 9 and 10, the subscript "0" refers to the fixed frame, whereas the fixed frame was labeled 1 in ref 7. Eventually, if the U_k^y values are zero, these expressions reduce to those in ref 7.

References and Notes

(1) Truhlar, D. G.; Isaacson, A. D.; Garrett, B. C. In *Theory of Chemical Reaction Dynamics*; Baer, M., Ed.; Chemical Rubber: Boca Raton, FL, 1985; Vol. 4.

(2) Steinfeld, J. I.; Francisco, J. S.; Hase, W. L. In *Chemical Kinetics and Dynamics*; Prentice Hall: Englewood Cliffs, NJ, 1989; Chapter 10.

(3) Intrinsic reaction coordinate (IRC) calculations are not practical for barrierless reactions since the gradient is zero for infinite separation of the reactants. Starting IRC calculations with selected configurations may result in arbitrarily choosing a reaction path. If this pathway is unique, IRC calculations yield this unique reaction path independently of the starting configuration. However, this is not true if multiple pathways are available to reactants. in this work, for example, the $Cl^{\bullet} + CH_2{=}CCl_2$ association reaction may lead to $^{\bullet}Cl\cdots CH_2{=}CCl_2$ or $CH_2{=}CCl_2\cdots Cl^{\bullet}$ intermediates via two different pathways, both of which are local minima on the PES.

(4) Knox, J. H. *Trans. Faraday Soc.* **1966**, *62*, 1206. Tardy, D. C.; Rabinovitch, B. S. *Trans. Faraday Soc.* **1968**, *64*, 1844.

(5) Yamada, T.; El-Sinawi, A.; Siraj, M.; Taylor, P. H.; Peng, J.; Hu, X.; Marshall, P. *J. Phys. Chem. A* **2001**, *105*, 7588.
(6) Pitzer, K. S.; Gwinn, W. D. *J. Chem. Phys.* **1942**, *10*, 428.
(7) Kilpatrick, J. E.; Pitzer, K. S. *J. Chem. Phys.* **1949**, *17*, 1064.
(8) Hase, W. L.; Mondro, S. L.; Duchovic, R. J.; Hirst, D. M. *J. Am. Chem. Soc.* **1987**, *109*, 2916. de Sainte Claire, P.; Hase, W. L. *Phys. Rev. B: Condens. Matter* **1997**, *56*, 13543.
(9) Robertson, S. H.; Wagner, A. F.; Wardlaw, D. M. *J. Chem. Phys.* **1995**, *103*, 2917.
(10) Rånby, B.; Rabek, J. F. In *ESR Spectroscopy in Polymer Research*; Springer-Verlag: Berlin, 1977.
(11) Hayashi, K.; Yonezawa, T.; Okamura, S.; Fukui, K. *J. Polym. Sci. A* **1963**, *1*, 1405.
(12) Giese, B. In *Radicals in Organic Synthesis: Formation of the Carbon−Carbon Bonds*; Baldwin, J. E., Ed.; Pergamon Press: Oxford, 1986.
(13) Améduri, B.; Boutevin, B. In *Telomerisation Reactions of Fluorinated Alkenes*; Chambers, R. D., Ed.; Topics in Current Chemistry; Springer: Heidelberg, 1997; Vol. 192, p 165.
(14) Fleming, G. L.; Haszeldine, R. N.; Tipping, A. E. *J. Chem. Soc., Perkin Trans.* **1973**, *1*, 574.
(15) Améduri, B.; Boutevin, B.; Kharroubi, M.; Kostov, G.; Petrova, P. *J. Fluorine Chem.* **1998**, *91*, 41.
(16) Anhudinov, A. K.; Ryazanova, R. M.; Sokolov, S. V. *J. Org. Chem. USSR* **1974**, *10*, 2520.
(17) Kremlev, M. M.; Moklyachuk, L. I.; Fialkov, Yu. A.; Yagupol'skiĭ, L. M. *Zh. Org. Khim.* **1984**, *20*, 1162.
(18) Hajek, M.; Kotora, M. *J. Fluorine Chem.* **1993**, *64*, 101.
(19) Costa, A. T. *J. Chem. Soc.* **1961**, 2995.
(20) Ashton, D. S.; Sand, D. J.; Tedder, J. M.; Walton, J. C. *J. Chem. Soc., Perkin Trans. II* **1975**, 320.
(21) Bissel, E. R. *J. Org. Chem.* **1964**, *29*, 252.
(22) Hucknall, D. J. In *Chemistry of Hydrocarbon Combustion*; Chapman and Hall: New York, 1985.
(23) Stolarski, R.; Bojkov, R.; Bishop, L.; Zerefos, C.; Staehelin, J.; Zawodny, J. *Science* **1992**, *256*, 342.
(24) Kerr, J. B.; McElroy, C. T. *Science* **1993**, *262*, 1032.
(25) Ravishankara, A. R.; Turnipseed, A. A.; Jensen, N. R.; Barone, S.; Mills, M.; Howard, C. J.; Solomon, S. *Science* **1994**, *263*, 71.
(26) Von Sonntag, C. In *The Chemical Basis of Radiation Biology*; Taylor & Francis: London, 1987; Chapter 6.
(27) Hoganson, W.; Babcock, G. T. *Biochemistry* **1992**, *31*, 11874.
(28) Tedder, J. M. *Angew. Chem., Int. Ed. Engl.* **1982**, *21*, 401.
(29) Giese, B. *Angew. Chem., Int. Ed. Engl.* **1983**, *22*, 753.
(30) Kharroubi, M.; Manseri, A.; Améduri, B.; Boutevin, B. *J. Fluorine Chem.* **2000**, *103*, 145.
(31) Braña, P.; Menéndez, B.; Fernández, T.; Sordo, J. A. *Chem. Phys. Lett.* **2000**, *325*, 693.
(32) Braña, P.; Menéndez, B.; Fernández, T.; Sordo, J. A. *J. Phys. Chem. A* **2000**, *104*, 10842.
(33) Sekušak, S.; Liedl, K. R.; Sabljić, A. *J. Phys. Chem. A* **1998**, *102*, 1584.
(34) Abbatt, J. P. D.; Anderson, J. G. *J. Phys. Chem.* **1991**, *95*, 2382.
(35) Atkinson, R.; Aschmann, S. M. *Int. J. Chem. Kinet.* **1987**, *19*, 1097.
(36) Sosa, C.; Schlegel, H. B. *J. Am. Chem. Soc.* **1987**, *109*, 7007.
(37) Aubanel, E. E.; Wardlaw, D. M. *J. Phys. Chem.* **1989**, *93*, 3117.
(38) Hase, W. L.; Wardlaw, D. M. In *Advances in Gas-Phase Photochemistry and Kinetics, Bimolecular Collisions*; Ashfold, M. N. R., Baggott, J. E., Eds.; Burlington House: London, 1989; p 171.
(39) McQuarrie, D. A. In *Statistical Thermodynamics*; University Science Books: Mill Valley, CA, 1973.
(40) This ratio was set to 0.5 here since the ground electronic state of the chlorine radical is $^2P_{3/2}$. The electronic partition function of the TS is 2.
(41) Aubanel, E. E.; Robertson, S. H.; Wardlaw, D. M. *J. Chem. Soc., Faraday Trans.* **1991**, *87*, 2291.
(42) Rempe, S. B.; Watts, R. O. *Chem. Phys. Lett.* **1997**, *269*, 455.
(43) Wagner, A. F.; Harding, L. B.; Robertson, S. H.; Wardlaw, D. M. *Ber. Bunsen-Ges. Phys. Chem.* **1997**, *101*, 391.
(44) Truhlar, D. G. *J. Comput. Chem.* **1991**, *12*, 266.
(45) Edinoff, M. L.; Aston, J. G. *J. Chem. Phys.* **1935**, *3*, 379.
(46) It should be pointed out that our computer program can treat the much more general case of a species with many coupled internal rotors. In this case, eq 6 does not hold and the product of external and internal rotation partition functions is proportional to the square-root of the full kinetic energy matrix determinant.
(47) Vande Linde, S. R.; Mondro, S. L.; Hase, W. L. *J. Chem. Phys.* **1987**, *86*, 1348.
(48) Korchowiec, J.; Uchimaru, T. *J. Phys. Chem. A* **1998**, *102*, 2439.
(49) Heuts, J. P.; Gilbert, R. G.; Radom, L. *J. Phys. Chem.* **1996**, *100*, 18997.
(50) Arnaud, R.; Bugeaud, N.; Vetere, V.; Barone, V. *J. Am. Chem. Soc.* **1998**, *120*, 5733.
(51) Bottoni, A. *J. Chem. Soc., Perkin Trans. 2* **1996**, *2041*.
(52) Wong, M. W.; Radom, L. *J. Phys. Chem. A* **1998**, *102*, 2237.
(53) Radom, L.; Wong, M. W.; Pross, A. In *Controlled Radical Polymerization*; Matyjaszewski, K., Ed.; ACS Symposium Series 685; American Chemical Society: Washington, DC, 1998; Chapter 2.
(54) Shaik, S. S.; Schlegel, H. B.; Wolfe, S. In *Theoretical Aspects of Physical Organic Chemistry, The S_N2 Transition State*; Wiley: New York, 1992.
(55) Shaik, S. S.; Canadell, E. *J. Am. Chem. Soc.* **1990**, *112*, 1446. Poblet, J. M.; Canadell, E.; Sordo, T. *Can. J. Chem.* **1983**, *61*, 2068.
(56) Donovan, W. H.; Famini, G. R. *J. Phys. Chem.* **1994**, *98*, 7811.
(57) Wong, M. W.; Pross, A.; Radom, L. *Isr. J. Chem.* **1993**, *33*, 415.
(58) Riehl, J.-F.; Musaev, D. G.; Morokuma, K. *J. Chem. Phys.* **1994**, *101*, 5942.
(59) Engels, B.; Peyerimhoff, S. D.; Skell, P. S. *J. Phys. Chem.* **1990**, *94*, 1267.
(60) Houk, K. N.; Paddon-Row, M. N.; Spellmeyer, D. C.; Rondan, N. G.; Nagase, S. *J. Org. Chem.* **1986**, *51*, 2874.
(61) Schlegel, H. B. *J. Phys. Chem.* **1982**, *86*, 4878. Schlegel, H. B.; Bhalla, K. C.; Hase, W. L. *J. Phys. Chem.* **1982**, *86*, 4883. Schlegel, H. B.; Sosa, C. *J. Phys. Chem.* **1984**, *88*, 1141. Sosa, C.; Schlegel, H. B. *J. Am. Chem. Soc.* **1987**, *109*, 4193.
(62) Frisch, M. J.; Trucks, G. W.; Schlegel, H. B.; Scuseria, G. E.; Robb, M. A.; Cheeseman, J. R.; Zakrzewski, V. G.; Montgomery, J. A., Jr.; Stratmann, R. E.; Burant, J. C.; Dapprich, S.; Millam, J. M.; Daniels, A. D.; Kudin, K. N.; Strain, M. C.; Farkas, O.; Tomasi, J.; Barone, V.; Cossi, M.; Cammi, R.; Mennucci, B.; Pomelli, C.; Adamo, C.; Clifford, S.; Ochterski, J.; Petersson, G. A.; Ayala, P. Y.; Cui, Q.; Morokuma, K.; Malick, D. K.; Rabuck, A. D.; Raghavachari, K.; Foresman, J. B.; Cioslowski, J.; Ortiz, J. V.; Baboul, A. G.; Stefanov, B. B.; Liu, G.; Liashenko, A.; Piskorz, P.; Komaromi, I.; Gomperts, R.; Martin, R. L.; Fox, D. J.; Keith, T.; Al-Laham, M. A.; Peng, C. Y.; Nanayakkara, A.; Gonzalez, C.; Challacombe, M.; Gill, P. M. W.; Johnson, B.; Chen, W.; Wong, M. W.; Andres, J. L.; Gonzalez, C.; Head-Gordon, M.; Replogle, E. S.; Pople, J. A. *Gaussian 98*, revision A.7; Gaussian, Inc.: Pittsburgh, PA, 1998.
(63) Heidrich, D. In *The Reaction Path in Chemistry: Current Approaches and Perspectives*; Heidrich, D., Ed.; Kluwer Academic Publishers: Dordrecht, The Netherlands, 1995.
(64) Rothman, M. J.; Lohr, L. L., Jr.; Ewig, C. S.; Van Wazer, J. R. In *Potential Energy Surfaces and Dynamics Calculations*; Truhlar, D. G., Ed.; Plenum: New York, 1981.
(65) Dainton, F. S.; Lomax, D. A.; Weston, M. *Trans. Faraday Soc.* **1962**, *58*, 308.
(66) Ken, J. A.; Parsonage, M. J. *Evaluated Kinetic Data on Gas-Phase Addition Reactions: Reactions of Atoms and Radicals with Alkenes, Alkynes and Aromatic Compounds*; Butterworths: London, 1972.
(67) Calculations with the CASSCF method were performed in our laboratory on $C_2H_2F_2$ (C_{2v} symmetry). This species was chosen because it has fewer electrons than $C_2H_2Cl_2$. The goal of this calculation was to select appropriate active orbitals in order to reproduce the QCISD(T) C═C bond length of 1.330 Å. Indeed, this bond undergoes key changes during the association reaction with a halogen radical. Including the highest occupied and lowest unoccupied molecular orbitals in the active space, π HOMO and π^* LUMO, respectively, resulted in a significantly shorter C═C bond length (1.315 Å) with respect to QCISD(T) results. Including the C═C σ and σ^* MOs in the active space resulted in much better agreement (1.331 Å). Thus a CAS(4,4) calculation (i.e., four electrons in four molecular orbitals: σ, π, σ^*, and π^*) was needed to get reliable energies for the reactant molecule. In the associated species, two of the valence p orbitals of the incoming halogen radical have the correct symmetry (those in the *yz* plane, see Figure 2). These should be included in the active space, thus resulting in four more orbitals and three extra electrons. Consequently, a CAS(7,8) calculation was the minimum level required to obtain an accurate potential energy surface. Such calculations, however, are beyond the scope of this work.
(68) Kleindienst, T. E.; Shepson, P. B.; Nero, C. M.; Bufalini, J. J. *Int. J. Chem. Kinet.* **1989**, *21*, 863.